

Prompt GeV emission in the synchrotron self-Compton model for Gamma-Ray Bursts

A. Panaitescu

Space Science and Applications, M S D 466, Los Alamos National Laboratory, Los Alamos, NM 87545, USA

ABSTRACT

The detection in 10 bursts of an optical counterpart emission (i.e. during the prompt GRB phase) that is 10^{-4} brighter than the extrapolation of the burst spectrum to optical frequencies suggests a synchrotron self-Compton origin for the GRB emission, synchrotron producing the optical counterpart emission. In this model, the second upscattering of the burst photons yields a prompt GeV (TeV) emission, whose brightness depends strongly on an unknown quantity, the peak energy of the primary synchrotron spectrum. Measurements of the optical, γ -ray, and GeV prompt fluxes can be used to test the synchrotron self-Compton model for GRBs and to determine directly the total radiative output of GRBs. For a set of 29 GRBs with optical counterpart detections, we find that the expected GeV photon flux should correlate with the fluence of the sub-MeV emission and anticorrelate with the brightness of the optical counterpart, the strength of these correlations decreasing for an increasing width of the synchrotron peak energy distribution. The detection of a GeV prompt emission consistent with the extrapolation of the burst spectrum to higher energies would rule out the synchrotron self-Compton model if the sub-MeV burst emission were very bright and the (intrinsic) optical counterpart were very dim.

Key words: radiation mechanisms: non-thermal – shock waves – gamma-rays: bursts

1 INTRODUCTION

The optical flux during the prompt γ -ray emission is 1{4 orders of magnitude larger than the extrapolation of the burst spectrum to optical for GRB 990123 (figure 2 of Galama et al 1999), GRB 061126 (figure 5 Perley et al 2008), GRB 080319B (figure 3 of Racusin et al 2008), and for GRBs 060111B, 060927, 061007, 061121, 071003, 080413, and 080810 (as can be inferred from the optical and GRB properties listed in Table 1). This may suggest that the optical and burst emissions arise from different radiation processes, synchrotron emission dominating the optical counterpart and inverse-Compton scatterings producing the 10 keV {10 MeV emission (model b2 of Meszaros & Rees 1997, Panaitescu & Meszaros 2000).

An essential assumption for the synchrotron self-Compton interpretation of GRBs is that the optical counterpart and burst emissions arise from the same relativistic ejecta. For GRB 080319B, whose optical counterpart emission was well-sampled (Karpov et al 2008), that assumption is supported by the broad correlation of optical and γ -ray prompt light-curves (Stamatikos et al 2008). A correlation between burst and optical counterpart emissions is also possible in the internal shock model (Rees & Meszaros 1994) for GRBs if the pair of reverse and forward shocks produced by the interaction of relativistic shells radiate in the optical and at sub-MeV, as was proposed by Yu, Wand & Dai (2008) for GRB 080319B. The latter model requires that,

for all pairs of interacting shells, the Lorentz factor ratio is very larger (above 1000), but it produces a weaker GeV emission from inverse-Compton scatterings than does the second upscattering of the former model. A tight correlation of GRB and optical counterpart fluctuations is not expected in either model, as the spectra of two emission components (synchrotron and inverse-Compton, or just synchrotron from reverse and forward shocks, respectively) may peak, sometimes, far from the corresponding observing band-passes (optical and γ -ray) and not yield a pulse in that photon range.

From the optical and γ -ray properties of the prompt emissions of GRB 080319B, Kumar & Panaitescu (2008) have inferred that the upscattering of GRB photons (i.e. the second inverse-Compton scattering of the primary synchrotron photons) should have produced a GeV photon yield over the burst duration of thousands of photons for Fermi's Large Area Telescope (LAT) and hundreds of photons for Agil's Gamma-Ray Imaging Detector (GRID), the second scattering GeV {TeV emission accompanying GRB 080319B containing 10 times more energy than released at sub-MeV by the first scattering. If the synchrotron self-Compton process were at work in other bursts with an optical counterpart dimmer than that of GRB 080319B, then the Compton parameter for the second scattering could be substantially larger than for GRB 080319B, leading to bursts that radiate much more energy in the GeV than at sub-MeV (Piran, Sari

& Zou 2008); however, synchrotron peak energies well from optical can reduce substantially the Compton parameter of the second scattering and its GeV flux.

Currently, the observational evidence for a prompt emission component peaking above 10 MeV (as is possible in the synchrotron self-Compton model for GRBs) is modest. The spectra of 15 GRBs measured by the Energetic Gamma-Ray Experiment Telescope (EGRET) calorimeter on the Compton Gamma-Ray Observatory up to 100 MeV (Kane et al 2008) show only 3 such cases. One of them is GRB 941017 (Gonzales et al 2003), whose F spectrum rises up to 100 MeV; the other ones are GRB 930506 and 980923. A prompt GeV flux that exceeds the extrapolation of the burst spectrum to higher energies has also been detected by EGRET for GRB 940217 (Hurley et al 1994). At the other end, the most notable evidence provided by EGRET for the absence of higher energy emission is for GRB 930131 (Sommer et al 1994), whose power-law spectrum extends up to 1 GeV. We also note that the prompt emissions above 100 MeV of two recent bursts measured by Fermi-LAT lie on the extrapolation of the MeV spectrum.

Double upscattering of the synchrotron emission is not the only model that can yield a prompt GeV emission. Previous proposed models for a prompt GeV emission include the more "mundane" synchrotron and inverse-Compton from internal shocks (e.g. Papathanassiou & Meszaros 1996), inverse-Compton emission from the reverse-shock (e.g. Granot & Gueta 2003) or from the forward-shock (e.g. Wang, Dai & Lu 2001), and upscattering of reverse-shock synchrotron photons in the forward-shock (Pe'er & Waxman 2004), as well as some more "exotic" and uncertain ones (e.g. synchrotron emission from ultra-high energy protons or the electrons and muons formed from by the photo-pion decay of those protons (Asano & Inoue 2007)). Evidently, a comparison of the optical, sub-MeV, and GeV emissions with model-expected correlations will be required to distinguish among the various process proposed for the higher energy component.

In this paper, we develop the formalism by which optical counterpart and prompt burst measurements can be used to infer the GeV flux accompanying GRBs and apply it to the bursts with optical counterpart measurements (detections or upper limits) to calculate the bolometric GRB output. As shown below, these quantities depend strongly on the peak energy of the primary synchrotron spectrum. The direct determination of that quantity through optical and near-infrared observations of the prompt emission and the measurement of the GeV prompt flux can then be used to test the synchrotron self-Compton model for GRBs. If the peak energy of the synchrotron spectrum cannot be determined observationally, then the GeV and optical fluxes and spectral slopes can be used to perform a weaker test of that model.

The following calculations for the synchrotron self-Compton emissions are general and do not depend on the dissipation mechanism (i.e. type of shock) which accelerates relativistic electrons and produces magnetic fields. It could be the external reverse shock which propagates into the relativistic ejecta, if that mechanism can account for the burst variability, or it could be internal shocks in a variable outflow, as was proposed by Sari & Piran (1999) and Meszaros & Rees (1999), respectively, to explain the bright optical

counterpart of GRB 990123. The physical parameters of the synchrotron self-Compton model required to account for the optical and sub-MeV emissions of that particular burst, GRB 990123, were inferred by Panaitescu & Kumar (2007). As for GRB 080319B, it was found that the peak energy of the synchrotron spectrum was not far from the optical.

2 FORMALISM

In the synchrotron self-Compton model for the GRB emission, the peak energy and peak flux of the first inverse-Compton scattering are the peak energy ϵ'' and flux F'' of the GRB spectrum. The peak energy ϵ_p and flux F_p of the primary synchrotron spectrum could be measured directly with robotic telescopes performing multiband observations of the optical counterpart only if ϵ_p falls in the optical band-pass (i.e. $\epsilon_p \approx 2$ eV), but otherwise remain unknown (optical counterpart measurements yield a relation between F_p and ϵ_p). Both quantities F_p and ϵ_p are needed to calculate the typical energy $\gamma m_e c^2$ of the radiating electrons and the optical thickness τ_e to electron scattering of the radiating medium, which, together with the F'' and ϵ'' of the first scattering, lead to the peak energy ϵ_{GeV} and flux F_{GeV} of the second inverse-Compton scattering. The last two quantities set the GeV prompt flux, thus observations by Fermi-LAT and AGILE-GRID of the GeV emission accompanying GRBs can be used in conjunction with the optical counterpart and burst measurements to test the synchrotron self-Compton model for GRBs. In this section, we relate the properties of the twice upscattered emission to those of the prompt optical and γ -rays.

The peak energy ϵ_{GeV} of the second inverse-Compton emission spectrum and the peak flux F_{GeV} at ϵ_{GeV} are related to those of the first inverse-Compton by

$$\epsilon_{GeV} = \frac{2}{p} \epsilon'' \quad F_{GeV} = \tau_e F'' \quad (1)$$

with $p = (\epsilon''/\epsilon_{peak})^{1/2}$ and $\tau_e = F''/F_{peak}$ relating the peak energies and flux of the first inverse-Compton spectrum to those of the spectrum of the received synchrotron emission, ϵ_{peak} and F_{peak} . If the emitting fluid is optically thin to synchrotron self-absorption at the peak energy ϵ_p of the synchrotron emissivity, then $\epsilon_{peak} = \epsilon_p$ and $F_{peak} = F_p$; however, if the optical thickness to synchrotron self-absorption at ϵ_p is above unity, the received spectrum peaks at the synchrotron self-absorption energy ϵ_a (i.e. $\epsilon_{peak} = \epsilon_a$). Thus

$$p = \begin{cases} (\epsilon''/\epsilon_p)^{1/2} & p < 1 \\ (\epsilon''/\epsilon_a)^{1/2} & p > 1 \end{cases}; \quad \tau_e = \begin{cases} F''/F_p & p < 1 \\ F''/F_a & p > 1 \end{cases} \quad (2)$$

where F_a is the synchrotron flux at ϵ_a and

$$\tau_e = \frac{5e}{eB} \frac{1}{p} \quad (3)$$

is the optical thickness to synchrotron self-absorption at the peak energy ϵ_p , σ_e being the cross-section for electron scattering (in the Thomson regime) and B the magnetic field strength. The value of B can be inferred from the synchrotron peak energy:

$$\epsilon_p = \frac{eh}{4m_e c} \frac{2B}{z + 1} \quad (4)$$

taking into account the relativistic boost of photon energy by the Lorentz factor γ of the source, which leads to

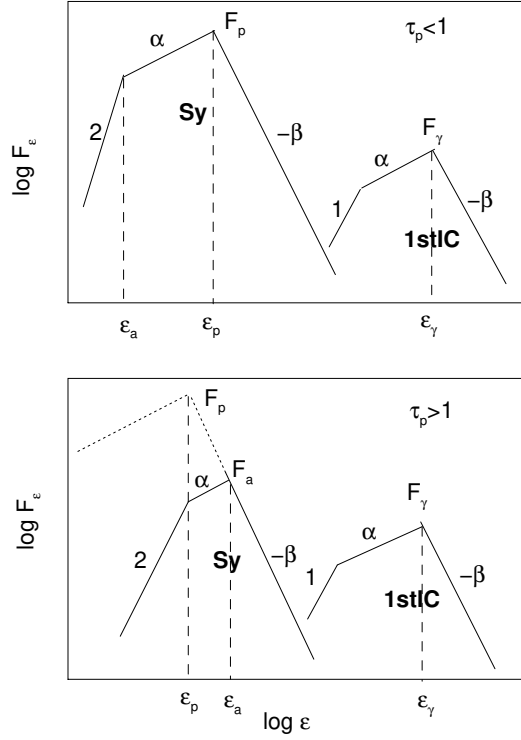


Figure 1. Power-law spectra of synchrotron and first inverse-Compton emissions for an emitting plasma which is optically thin ($\tau_p < 1$, upper panel) and optically thick ($\tau_p > 1$, lower panel) at the emissivity peak energy ϵ_p , and for electrons with a power-law energy distribution above that corresponding to the synchrotron characteristic energy ϵ_p . Spectral power-law indices ($d \log F = d \log \epsilon$) are indicated. Below the peak of the spectrum, the slopes are $\alpha = 1/3$ and $\beta = 5/2$ for $\tau_p < 1$ and $\tau_p > 1$, respectively. However, we allow an arbitrary slope $\alpha < 1/3$ ($\beta = 5/2$) to accommodate the diversity of low-energy slope measured for the GRB emission (which is the first inverse-Compton component), which may be due to a more complex electron distribution than a pure power-law only above ϵ_p . GRB observations determine the peak energy and flux (ϵ_p, F_p) of the first inverse-Compton emission, while optical counterpart measurements set a constraint on the spectral peak properties (ϵ_p, F_p) of the synchrotron emission which depends on the location of the optical bandpass relative to the break energies ϵ_p (emissivity peak) and ϵ_a (self-absorption).

$$\epsilon_p = \frac{52.6 \text{ MeV}}{\epsilon_p} \frac{e}{(z+1)^{3/2}} : \quad (5)$$

Therefore, to find ϵ_p and ϵ_a , the quantities $\epsilon_p, \epsilon_a, F_p$, and F_a must be constrained from the counterpart optical flux (which is the only measurable quantity directly pertaining to the synchrotron emission). As that provides only one constraint, we shall express the following results as function of the peak energy ϵ_p , and consider separately the $\tau_p < 1$ and $\tau_p > 1$ cases.

For $\tau_p < 1$, equations (2) and (5) yield

$$\epsilon_p = k \frac{F_p}{F_a} \epsilon_p^{1/2} ; \quad k = \frac{52.6 \text{ MeV}}{(z+1)^{3/2}} : \quad (6)$$

In this case, the self-absorption energy is

$$\epsilon_a = \epsilon_p^{3/5} < \epsilon_p \quad (7)$$

and the optical counterpart flux F_o is (Figure 1, upper panel)

$$F_o = F_p \begin{cases} (\epsilon_o = \epsilon_a)^2 (\epsilon_a = \epsilon_p) & \epsilon_o < \epsilon_a < \epsilon_p \\ (\epsilon_o = \epsilon_p) & \epsilon_a < \epsilon_o < \epsilon_p \\ (\epsilon_p = \epsilon_o) & \epsilon_a < \epsilon_p < \epsilon_o \end{cases} \quad (8)$$

where α and β are the spectral slopes below and above ϵ_p of the synchrotron emissivity, which are the same as low and high energies slope of the first inverse-Compton GRB spectrum: F_p / ϵ_p^α and F_p / ϵ_p^β , respectively. Substituting F_p in equation (9) and using equation (7), one finds

$$\epsilon_p = k \frac{F_p}{F_o} \frac{\epsilon_o^{3/2}}{\epsilon_p^{3/2}} : \quad (9)$$

for the $\epsilon_o < \epsilon_a < \epsilon_p$ case. Then, the starting condition $\tau_p < 1$ is equivalent to $\epsilon_p > \epsilon_1$ with

$$\epsilon_1 = (k^0 \epsilon_o^{3/2})^{2/3} ; \quad k^0 = \frac{F_o}{k F_p} \quad (10)$$

while the assumption $\epsilon_o < \epsilon_a$ is equivalent to $\epsilon_p > \epsilon_2$ with

$$\epsilon_2 = (k^0 \epsilon_o^{3/2})^{6/5} : \quad (11)$$

For the $\epsilon_a < \epsilon_o < \epsilon_p$ case, one obtains

$$\epsilon_p = k \frac{F_p}{F_o} \frac{\epsilon_o}{\epsilon_p^{1/2}} \quad (12)$$

while for the $\epsilon_a < \epsilon_p < \epsilon_o$ case

$$\epsilon_p = k \frac{F_p}{F_o} \frac{\epsilon_p^{1/2}}{\epsilon_o} \quad (13)$$

the $\tau_p < 1$ condition requiring that $\epsilon_p < \epsilon_3$, where

$$\epsilon_3 = (k^0 \epsilon_o)^{2/(2+1)} : \quad (14)$$

The three reference photon energies ϵ_1, ϵ_2 , and ϵ_3 depend only on observables and allow the selection of the photon energy ordering given in equation (8):

$$\begin{cases} \epsilon_o < \epsilon_a < \epsilon_p & \text{if } \epsilon_1, \epsilon_2 < \epsilon_p \\ \epsilon_a < \epsilon_o < \epsilon_p & \text{if } \epsilon_o < \epsilon_p < \epsilon_1 \\ \epsilon_a < \epsilon_p < \epsilon_o & \text{if } \epsilon_p < \epsilon_3, \epsilon_o \end{cases} \quad (15)$$

Thus, given a peak energy ϵ_p , equation (15) identifies the ordering of ϵ_o, ϵ_a , and ϵ_p , from where ϵ_p can be determined using equations (9), (16), or (13), further leading to ϵ_a through equation (7), then to the peak flux F_p of equation (8), then to the ϵ_e of equation (2) and, finally, to the spectral peak flux of the second inverse-Compton scattering of equation (1) as a function of ϵ_p .

For $\tau_p > 1$, we are interested in calculating the self-absorption energy ϵ_a and the synchrotron flux F_a at ϵ_a as a function of ϵ_p . From equations (2) and (5), one obtains

$$\epsilon_p = k \frac{F_p}{F_a} \frac{\epsilon_a^{3/2}}{\epsilon_p^{3/2}} \quad (16)$$

with ϵ_a being

$$\epsilon_a = \epsilon_p^{2/5} > \epsilon_p : \quad (17)$$

The optical counterpart flux is related to F_a through (Figure 1, lower panel)

$$F_o = F_a \begin{cases} (\epsilon_o = \epsilon_p)^2 (\epsilon_p = \epsilon_a) & \epsilon_o < \epsilon_p < \epsilon_a \\ (\epsilon_o = \epsilon_a) & \epsilon_p < \epsilon_o < \epsilon_a \\ (\epsilon_a = \epsilon_o) & \epsilon_p < \epsilon_a < \epsilon_o \end{cases} \quad (18)$$

Continuing in a similar way as shown above for $p < 1$, one finds that the ordering of energies in equation (18) is set by ν_p as following

$$\begin{cases} \nu_o < \nu_p < \nu_a & \text{if } \nu_o < \nu_p < \nu_2 \\ \nu_p < \nu_o < \nu_a & \text{if } \nu_4 < \nu_p < \nu_o \\ \nu_p < \nu_a < \nu_o & \text{if } \nu_3 < \nu_p < \nu_4 \end{cases} \quad (19)$$

where

$$\nu_4 = (k^0 \nu_o^{+1})^{2=(2+3)}; \quad (20)$$

Then, the optical thickness to self-absorption at the spectral peak of the synchrotron emission is

$$\begin{aligned} \tau &< (k^2 \nu_o^{3=2})^{(5+2)=(+1)} & \nu_o < \nu_p < \nu_a \\ p &= (k^0 \nu_o^{1=2})^{(5+2)=(+1)} & \nu_p < \nu_o < \nu_a \\ &: (k^0 \nu_p^{1=2} = \nu_o)^{+5=2} & \nu_p < \nu_a < \nu_o \end{aligned} \quad (21)$$

Equations (21), (17), and (18) allow the calculation of ν_a (ν_p) and F_a (F_p).

The reference energies ν_1 , ν_2 , ν_3 , and ν_4 have the same form $\nu(x) = (k^0 \nu_o^x)^{2=(2x+1)}$ with $x = 2; \frac{5}{3}; +1$, respectively, thus $\nu(x)$ has a singularity at $x = -1/2$. For $k^0 < \nu_o^{1=2}$, i.e. $F_o = F < (z+1)\nu_o^{3=2} = (52.6 \nu_o^{1=2} \text{ MeV})$, it can be shown that $d\nu(x)/dx > 0$ and the reference energies ordering is $\nu_3 < \nu_4 < \nu_o < \nu_1$ (the relative location of ν_2 depending on ν_p). For $k^0 > \nu_o^{1=2}$, $d\nu(x)/dx < 0$ and $\nu_1 < \nu_o < \nu_4 < \nu_3$.

The Klein-Nishina effect on the second inverse-Compton scattering is important if the energy of the first scattering (GRB) photon, as measured in the electron frame, is comparable or larger than the electron rest-mass energy, i.e. if $(z+1)(\nu_p) > m_e c^2$, where the typical electron Lorentz factor p is obtained using equation (2). Considering only the $p < 1$ case, for which $p = (\nu_p / \nu_o)^{1=2}$, implies that the Klein-Nishina effect is important for $\nu_p < \nu_{kn}$ with

$$\nu_{kn} = \frac{z+1}{m_e c^2} \nu_o^3 = 3 \frac{\nu_o}{200 \text{ keV}}^3 \frac{z+1}{3} \frac{1}{300} \text{ eV} \quad (22)$$

Thus, the Klein-Nishina effect is expected to be important only if the peak energy of the synchrotron spectrum is below optical. In this case, the energy of the twice up-scattered photon is $\nu_{GeV} = m_e c^2 p = (z+1)$ (lower than given in equation 1) and the peak flux of the second inverse-Compton emission is diminished by the decreased scattering cross-section, $\sigma_{e, kn} / \sigma_e (\nu_p = \nu_{kn})^{1=2} < \sigma_e$. For $\nu_a < \nu_p < \nu_o$, equations (8) and (2) lead to $\nu_e = (F/F_o)(\nu_p/\nu_o)$, and the Compton parameter for the second scattering is $Y_{GeV} = \sigma_{e, kn} \nu_{GeV} / \sigma_e = (\nu_p/\nu_{kn})^2$.

For ν_p above optical, the Klein-Nishina effect is negligible and $Y_{GeV} = Y = (F/F_o) = (F_p/F_p)$, where Y is the Compton parameter for the first scattering and F_p is given by equation (8) for $\nu_a < \nu_o < \nu_p$. Thus, the fluence of the twice up-scattered emission, $\nu_{GeV} = Y_{GeV}$, is

$$\begin{aligned} \nu_{GeV} &= \frac{2}{t F_o} \gtrsim \frac{m_e c^2}{z+1} \frac{1}{\nu_o^3} \frac{\nu_p}{\nu_o} & \nu_p < \nu_{kn} \\ &\gtrsim \frac{\nu_o}{\nu_p^{+1}} & \nu_{kn} < \nu_p \end{aligned} \quad (23)$$

where ν_o and t are the GRB fluence and duration, respectively.

Therefore, for fixed properties of the prompt optical and GRB emissions, the fluence of the GeV emission and

its Compton parameter increase as ν_p for $\nu_p < \nu_{kn}$ and decrease as $\nu_p^{-(+1)}$ for $\nu_p > \nu_{kn}$, being maximal when the peak energy of the synchrotron spectrum is in or close to the optical ($\nu_p = \nu_{kn} / \nu_o$). Using equation (23) to assess the effect of observables on the expected fluence of the second scattering, it could be expected that the GeV fluence is (1) correlated with the burst fluence (which is quite trivial, as the GeV photons are the upscattered burst photons) and (2) anticorrelated with the optical counterpart flux, burst duration, and peak energy of the GRB spectrum (if ν_p is below optical), with the caveats that these correlations (a) should be weakened and could be even wiped out by variations in ν_p from burst to burst (as ν_p affects strongly the GeV flux), (b) could be affected by correlations among optical and burst properties.

Figure 2 shows the dependence of some characteristics of the second inverse-Compton scattering (peak energy $\nu_{GeV} = \frac{2}{p} \nu_p$ and upscattered self-absorption frequency $\nu_a = \frac{4}{p} \nu_a$ in the upper panel, Compton parameter $Y_{GeV} = (\nu_{GeV} F_{GeV}) / (F)$ in the mid panel) on the peak energy ν_p of the synchrotron spectrum, calculated with the aid of the equations above. A side from the unknown ν_p , the optical and GRB spectral peak fluxes, F_o and F , are the other major factors affecting the brightness of the twice upscattered emission, the other parameters and observables having a lesser effect.

The GeV emission spectrum has the same shape as given in equations (8) and (18), except that upscattering of the self-absorbed part of the synchrotron spectrum yields a flatter one, F_ν / ν (Panaitescu & Meszaros 2000). Middle panel of Figure 2 shows the expected behaviour of the second scattering's Compton parameter, peaking for $\nu_p \sim 1 \text{ eV}$. As Y_{GeV} is a measure of the GeV fluence, it follows that a measurement of the prompt GeV fluence yields two solutions for the unknown peak ν_p of the synchrotron spectrum (see also equation 23). The real solution can be found using the 100 GeV spectrum: a hard F_ν / ν spectrum (resulting from up-scattering twice synchrotron photons below self-absorption) or one of slope up to tens of GeV indicates that $\nu_p < 1 \text{ eV}$, while a soft spectrum of slope above 10 GeV is expected for $\nu_p > 10 \text{ eV}$. Then, compatibility with the spectrum of the optical counterpart emission, which the bottom panel of Figure 2 shows that should be optically thin for $\nu_p < 1 \text{ eV}$ and thick for $\nu_p > 1 \text{ eV}$, offers a possible test of the synchrotron self-Compton model for the burst emission. A stronger test can be done if the peak energy of the GeV spectrum is measured, as in this case the GeV peak energy and fluences provide two independent constraints on the peak energy of the synchrotron spectrum.

3 APPLICATION TO BURSTS WITH OPTICAL COUNTERPART MEASUREMENTS

Without knowing the peak energy of the synchrotron spectrum, we proceed to estimate the GeV output and total energetics of bursts for which optical counterpart measurements exist for $\nu_p = 1 \text{ eV}$, which maximizes the GeV prompt output, and for $\nu_p = 0.01 \text{ eV}$ (values above optical also reduce the GeV output, with an upper limit of 100 eV on ν_p is imposed by requiring that the 10 keV prompt emission is

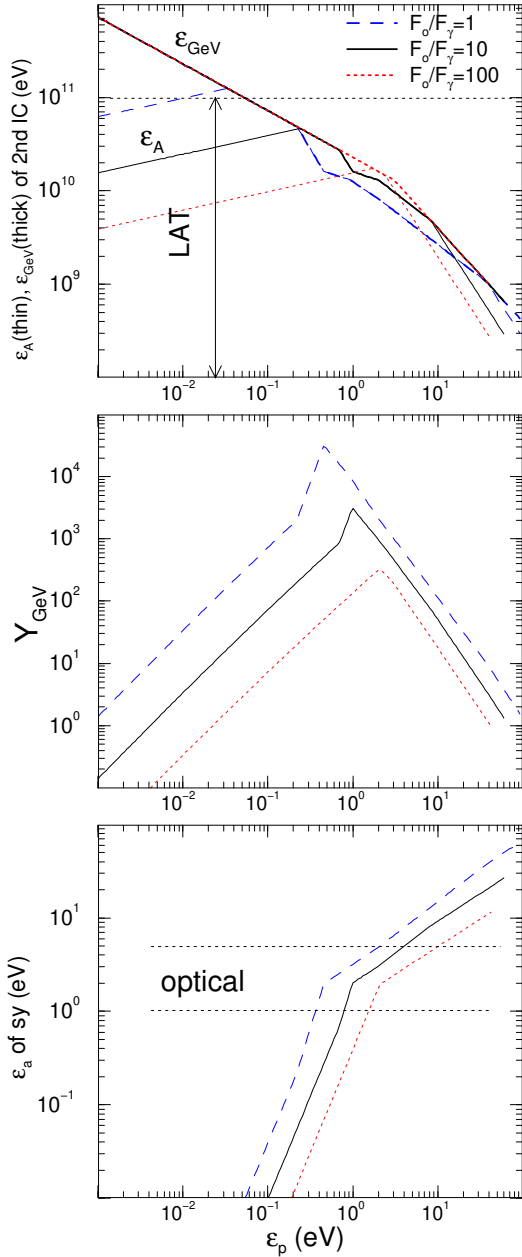


Figure 2. Dependence of twice up-scattered self-absorption ϵ_A and peak photon energy ϵ_{GeV} (top panel), Compton parameter for second scattering Y_{GeV} (mid panel), and synchrotron self-absorption energy ϵ_a (bottom panel) on the peak energy ϵ_p of the synchrotron emissivity, for three likely ratios of the (synchrotron) optical counterpart flux F_o to the (first inverse-Compton) GRB flux F_γ at the peak of GRB spectrum. Other parameters are set to average values for the GRBs of Table 1 for which optical counterpart measurements have been obtained: $F = 0.3$ mJy, GRB peak energy $\epsilon = 200$ keV (low and high-energy GRB spectral slopes $\alpha = 0$ and $\beta = 1.5$ were assumed), for calculation of Klein-Nishina effect on the upscattered emission: redshift $z = 2$ and a source Lorentz factor $\Gamma = 300$ was assumed. The ϵ_p is upper limited by the condition that the 10 keV (lower bound of bandpass of most burst detectors) flux is dominated by the first inverse-Compton component.

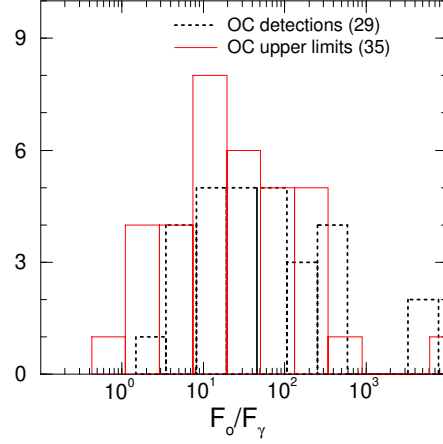


Figure 3. Distribution of optical counterpart flux to GRB spectral peak flux ratio for bursts with optical counterpart measurements (listed in Table 1). For more than half of bursts, only upper limits on the optical counterpart flux have been obtained, which sets an upper limit on the F_o/F_γ ratio, leading to a lower limit on the Compton parameter of the second scattering and on the GeV emission. For the bursts without a determined GRB peak energy ϵ , we assumed $\epsilon = 200$ keV, which is the average value for the bursts of Table 1 with measured ϵ .

dominated by the first scattering and not by the high-energy tail of the synchrotron spectrum).

The relevant properties of the optical and GRB prompt emissions of bursts with optical counterpart measurements are listed in Table 1. For more than half of those bursts, only upper limits on the optical counterpart flux have been obtained, the upper limit listed in Table 1 one being the deepest available and over an integration time that is within the burst emission or up to a factor two in time after the last GRB peak. Optical counterpart measurements have been corrected for the often modest Galactic dust extinction (given in last column), but may be affected by a more substantial extinction in the host galaxy that could be estimated, in some cases, from the optical afterglow spectrum.

The average optical flux for the 35 upper limits of Table 1 is 1 mJy, while that of the 19 counterpart detections 3 mJy, thus upper limits are, on average, 1 mag deeper than detections, but both averages have large dispersions (2.8 and 1.6 mag, respectively). The burst spectral peak energy ϵ has been measured for 27 of the GRBs in Table 1, the average being $\epsilon = 210$ keV with a dispersion of 0.45 dex. For those bursts, the flux F at the peak, calculated from the GRB fluence and spectrum (if not known, the low-energy GRB spectral slope was assumed to be $\alpha = 0$; the high-energy spectral slope at $\epsilon > \epsilon$ was set at $\beta = 1.5$), has an average $F = 0.3$ mJy with a dispersion of 0.5 dex. To calculate the GeV output for all bursts, we assume the average ϵ for the 37 burst without a reported peak energy. The average optical to GRB peak flux ratio, F_o/F_γ , which is an important parameter for the calculation of the GeV emission flux, is about the same for the bursts with known ϵ ($F_o/F_\gamma = 30$) as for those with assumed $\epsilon = \epsilon$ ($F_o/F_\gamma = 15$), as can be seen in Figure 3.

Table 1. Gamma-ray (columns 3-7) and optical (counterpart in column 8, afterglow in columns 9 and 10) properties of GRBs with optical counterpart measurements. t = burst duration, t_b = burst uence, E_p = GRB peak energy, α = slope of GRB spectrum below E_p (F_α / F_p). For GRBs in boldface, the optical counterpart flux is more than 10 times larger than the extrapolation of the GRB spectrum to optical energies. "W h" is for UVOT's white filter, "Un" for unfiltered.

GRB	redshift	t (s)	F_p (cgs)	band (keV)	E_p (keV)	α (keV)	OC ux (mag)	t_b (d)	decay index	E (B-V)
080810	3.35	140	1.7e-5	20-1000	-0.2	550	Un= 13.2	> 5.6	1.40	0.03
080802		176	1.3e-6	15-150	-0.8		W h> 20			0.80
080607	3.04	85	8.9e-5	20-4000	-0.1	420	R= 15.2	> 0.6		0.02
080603B	2.69	70	4.5e-6	20-1000	-0.2	100	Un= 14.1	0.6	3.05	0.01
080413	2.44	55	4.8e-6	15-1000	-0.2	170	Un= 12.8	> 0.15	1.2	0.16
080319B	0.94	57	5.7e-4	20-7000	0.2	650	V= 6.0	> 20	1.33	0.01
080310	2.43	365	2.3e-6	15-150		< 30	R= 17	2	2.4	0.04
080307		64	7.3e-7	15-150	-0.4		R> 16.9	> 0.06	0.7	0.03
080229		64	9.0e-6	15-150	-0.9		R> 14.7			0.15
080212		123	2.9e-6	15-150	-0.6		R> 17.8	> 0.6	0.4	0.16
080205		107	2.1e-6	15-150	-1.1		Un= 18.1			0.09
071031	2.69	180	9.0e-7	15-150		< 30	R= 15	> 0.13	0.55	0.01
071025		109	6.5e-6	15-150	-0.8		R> 17.3	> 0.2	1.8	0.08
071011		61	2.2e-6	15-150	-0.4		R> 16.9	> 0.15	0.7	0.91
071003	1.60	30	1.2e-5	20-4000	0.1	800	Un= 12.8	> 7.9	1.60	0.15
070808		32	1.2e-6	15-150	-0.5		Un> 16.2			0.02
070721B	3.63	32	2.1e-6	15-150	-0.3		W h= 15.9			0.02
070621		40	4.3e-6	15-150	-0.6		Un> 16.6			0.05
070616		402	1.9e-5	15-150	-0.9	100	V= 16.5			0.40
070521	0.55	55	1.8e-5	20-1000	0.1	220	R> 17.1			0.03
070429		163	9.2e-7	15-150	-1.1		Un> 16.2			0.17
070420		120	2.6e-5	20-1000	-0.1	170	R= 16.2	> 0.15	0.88	0.52
070419B		91	1.1e-5	100-1000	0.1		W h> 18.5			0.09
070419A	0.97	116	5.6e-7	15-150		< 30	R> 18.6	> 3.7	0.99	0.03
070411	2.95	101	2.5e-6	15-150	-0.7		R= 17.9	> 5.8	1.11	0.29
070306	1.50	210	5.5e-6	15-150	-0.7		W h> 19.8			0.03
070220		30	1.1e-5	20-2000	-0.2	300	W h> 19.6			0.90
070208	1.17	48	4.3e-7	15-150	-1.0		Un> 18.7	> 0.3	0.55	0.01
070129		460	3.1e-6	15-150	-1.0		V> 17.3			0.14
061222		100	2.7e-5	20-2000	0.1	280	Un> 17.0			0.10
061126	1.16	25	2.0e-5	30-2000	0.1	935	R= 12.93	> 1.8	0.99	0.18
061121	1.31	81	1.4e-5	15-150	0.2	455	Un= 14.9	> 3.9	1.05	0.05
061110	0.76	41	1.1e-6	15-150	-0.7		Un> 16.2			0.09
061007	1.26	90	2.5e-4	20-10000	0.3	400	Un= 13.6	> 1.7	1.70	0.02
060927	5.47	23	1.1e-6	15-150	0.1	70	Un= 16.5	> 2.6	1.01	0.06
060904B	0.70	192	1.7e-6	15-150	-0.7		Un= 17.3	> 1.9	1.02	0.17
060904A		80	1.6e-5	10-2000	0.1	160	R> 16.5			0.02
060814	0.84	134	2.7e-5	20-1000	-0.4	260	W h> 19.7			0.04
060729	0.54	116	2.7e-6	15-150	-0.9		Un= 15.67	> 28	1.27	0.05
060719		55	1.6e-6	15-150	-1.0		z> 16.6			0.07
060714	2.71	115	3.0e-6	15-150	-1.0		W h= 19.2	> 3.3	1.22	0.08
060607	3.08	100	2.6e-6	15-150	-0.5		r= 16.3	> 0.3	1.20	0.03
060602	0.79	60	1.6e-6	15-150	-0.1		R> 15			0.03
060507		185	4.1e-6	15-150	-0.8		Un> 15.5			0.16
060418	1.49	44	1.6e-5	20-1100	-0.5	230	z= 15.3	> 1.2	1.25	0.22
060312		43	1.8e-6	15-150	-0.4		R> 14.6			0.19
060210	3.91	255	7.7e-6	15-150	-0.5		R> 17.5			0.09
060124	2.30	710	2.8e-5	20-2000	-0.3	335	V= 17.08	> 6.2	1.42	0.14
060111B		25	5.6e-8	100-1000	-0.5		R= 13.8			0.10
051117		140	4.6e-6	15-150	-0.8		V= 20.0			0.02
051111	1.55	31	8.4e-6	100-700	-0.5		R= 13.2	> 1.0	1.62	0.16
051022	0.80	200	2.6e-4	20-2000	-0.2	510	R> 17.4			0.07
051001		190	1.8e-6	15-150	-1.1		R> 16.2			0.02
050915		53	8.8e-7	15-150	-0.4		R> 17.4			0.03
050904	6.29	225	5.4e-6	15-150	-0.4	340	R= 18.5	> 5.3	1.15	0.06
050822		102	3.4e-6	15-350		< 30	R> 16.6			0.02
050714		40	6.2e-7	20-200			R> 16.6			2.09
050713		70	9.1e-6	15-350	-0.6	310	R> 17.7	> 0.8	0.66	0.41
050520		80	2.4e-6	20-200			R> 16.1			0.02
050504		80	1.5e-6	20-200			R> 16.0			0.01
050408	1.24	34	1.9e-6	30-400			Un> 14.7	> 5.1	0.70	0.03
050319	3.24	10	8.0e-7	15-350	-1.2		R= 16.16	> 3.4	0.48	0.01
041219		540	1.0e-4	15-200			R> 19.4	> 1.0	1.2	1.75
990123	1.61	63	5.1e-4	20-1000	0.2	720	R= 8.95	2.0	1.65	0.02

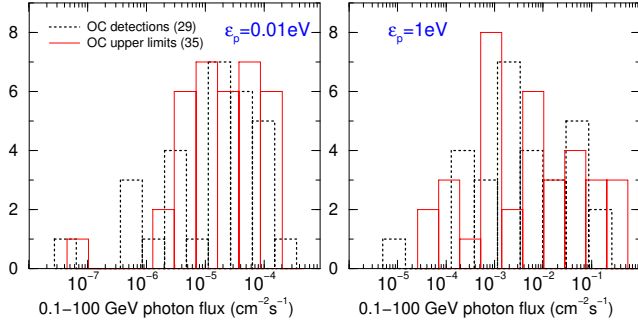


Figure 4. Distribution of the prompt 0.1-100 GeV photon flux resulting from the second scattering of the primary synchrotron emission, for two values of the peak energy ϵ_p of the synchrotron emissivity, and for the optical counterpart and γ -ray prompt emission properties of the bursts listed in Table 1. Upper limits on the optical counterpart flux set lower limits on the GeV flux. For the Fermi-LAT area of 5000 cm^2 and a burst lasting for 100 s (the average of the durations given in Table 1), the photon fluxes shown in left panel correspond to $0.2(50 \text{ GeV photons collected during the burst, while those in the right panel to } 10^{-10^5}$ prompt GeV photons. The effect of photon-photon attenuation, which depends strongly on the source Lorentz factor and radius where the prompt emission is released, is expected to be negligible for $\epsilon_p = 0.01 \text{ eV}$ (left panel), but could completely suppress the GeV photon flux for $\epsilon_p = 1 \text{ eV}$ (right panel) if the source radius is less than about 10^{16} cm .

3.1 Expected GeV prompt flux

Using the equations of the previous section, we calculate the break energies of the twice upscattered prompt emission and the peak flux of the GeV spectrum, and integrate over the power-law piecewise spectrum to obtain the 0.1-100 GeV prompt photon flux expected for the bursts of Table 1 in the synchrotron self-Compton model. The distribution of the resulting GeV fluxes is shown in Figure 4 for two values of ϵ_p . For its collecting area of thousands of cm^2 , the LAT onboard the Fermi satellite would detect hundreds to tens of thousands of photons during a 100 s burst if the peak energy of the synchrotron spectrum were at $\epsilon_p = 1 \text{ eV}$. However, the received GeV photon flux can be greatly affected by photon-photon attenuation, which depends primarily on the source radius R . Calculations show that, for the bursts of Table 1, photon-photon attenuation is negligible if $R > 10^{16} \text{ cm}$, but suppresses the 0.1-100 GeV flux above $\epsilon_p = 6 \cdot 10^{-3} (F_0 = 1 \text{ mJy})^{0.6} (F = 1 \text{ mJy})^{-1.5} (R = 10^{15} \text{ cm})^2 \text{ eV}$ if $R < 10^{16} \text{ cm}$. Thus, the non-detection of a GeV prompt emission produced by the second scattering may be due to either (1) an intrinsically weak GeV output, when ϵ_p is well below optical, in which case pair-formation is negligible, or (2) photon-photon attenuation suppressing the intrinsically-bright GeV emission produced when ϵ_p is close to the optical.

Fermi-LAT has received more than 10 photons above 1 GeV during GRB 080916C (Tajima et al 2008) and a similar number of photons below 1 GeV during GRB 080825C (Bouvier et al 2008). Optical counterpart measurements are not available for these bursts but the distributions shown in Figure 4 suggest that ϵ_p was in the 0.01-1 eV range, as a burst-integrated flux of 10 photons corresponds to $< 10^{-4} \text{ photons cm}^{-2} \text{ s}$, which is at the bright end of the dis-

tribution shown for $\epsilon_p = 0.01 \text{ eV}$ (left panel) and at the dim end for $\epsilon_p = 1 \text{ eV}$ (right panel). In fact, the above range for ϵ_p set by GeV observations of 080916C and 080825C is an upper limit because the measured high-energy fluxes are consistent with the extrapolation of the sub-MeV burst spectrum to GeV, as can be shown using the burst energies and high energy spectral slope reported by van der Horst & Goldstein (2008).

From equation (23), correlations are expected between the prompt GeV energy E_{GeV} and optical or GRB prompt emission properties (optical flux F_0 , GRB energy E , burst peak energy ϵ), provided that the peak energy ϵ_p of the synchrotron spectrum has a narrow distribution. For the 29 bursts of Table 1 with optical counterpart measurements, we find a significant correlation only between the expected GeV energy and the observed sub-MeV energy if ϵ_p is above optical (linear correlation coefficient $r(\log E_{\text{GeV}}; \log \epsilon) = 0.75$ corresponding to a 10^{-6} probability of a chance correlation), with other expected correlations being much less significant, owing to the scatter in the optical and GRB properties and to correlations among them. The strongest such correlation found is that between the burst energy and burst peak energy $r(\log E; \log \epsilon) = 0.70$, with best fit $\chi^2/\nu = 2.0$ which weakens the expected GeV correlation for ϵ_p is below optical, as in this case $E_{\text{GeV}} / \epsilon = 3$ (equation 23). Other correlations that we found among the prompt optical and GRB properties and which have a probability for a chance occurrence less than 10 percent are the optical counterpart flux F_0 (1) correlation with the burst energy E , (2) anticorrelation with burst duration t , both of which weaken the GeV F_0 anticorrelation expected from equation (23), and (3) correlation with GRB peak energy ϵ , which strengthens the expected GeV F_0 anticorrelation.

To assess the effect of ϵ_p not being universal on the expected correlations, we assume that, for the 29 bursts of Table 1 with optical counterpart measurements, $\log \epsilon_p$ has a uniform distribution between 0.01 eV and 100 eV, and find that such a distribution of ϵ_p among bursts weakens the GeV correlation found for a universal ϵ_p above optical, the linear correlation coefficient $r(\log E_{\text{GeV}}; \log \epsilon) = 0.2(0.3)$, corresponding to a 10(30) percent of a chance correlation. We conclude that, if the synchrotron self-Compton model for the GRB emission is correct, then the measured, prompt GeV energy (produced by the second upscattering) is likely to be correlated with the burst energy, and less likely to be correlated with other properties of the prompt emission (e.g. optical counterpart flux), but we note that the strength of this conclusion depends on the actual width of the synchrotron peak energy distribution.

3.2 Burst energetics

For bursts with known redshift, the isotropic radiative output E_r (synchrotron + 1st inverse Compton + 2nd inverse-Compton) can be calculated from the total prompt energy $E = E_{\text{syn}} + E_{\text{IC1}} + E_{\text{IC2}} = (Y^{-1} + 1 + Y_{\text{GeV}}) E_{\text{GeV}}$, with the GRB energy E_{GeV} in the 10 keV-10 MeV range calculated from the

² The E correlation was first noticed by Lloyd, Petrosian & Malozzi (2000), who suggested that it arose from a correlation of intrinsic source properties (see also Amati et al 2000)

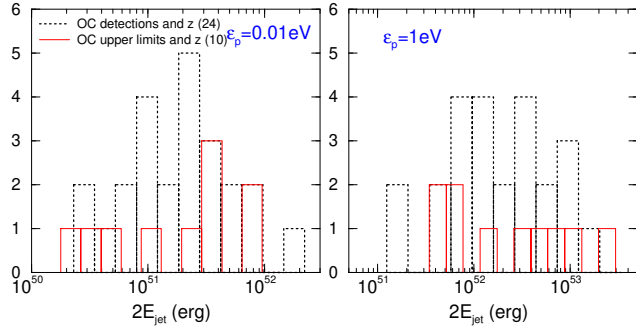


Figure 5. Distribution of lower limits on the collimation-corrected outflow initial energy (assuming a two-sided jet), for the optical counterparts and GRB prompt emission properties of Table 1, and for two possible values of the peak energy ϵ_p of the synchrotron emissivity. A radiative efficiency (ϵ_r) for the prompt emission of 50 percent was assumed. The lower limit on the jet opening was determined from the latest epoch t_b (Table 1) until which the optical afterglow light-curve decay does not exhibit the steepening expected from “seeing” the jet boundary, and assuming that the ambient medium has the typical density expected for a Wolf-Rayet progenitor of long bursts. Whenever it cannot be determined through afterglow observations, $t_b = 1$ day was assumed. (The jet energy has a moderate dependence on these parameters: $E_j / (t_b = 1)^{1/2}$.) Only the bursts of Table 1 with known redshift have been used and $\epsilon = 200$ keV was assumed when not known. Compared to the $\epsilon_p = 1$ eV case (right panel), the required jet energy is found to decrease by a factor 10 for a factor 100 increase or decrease in ϵ_p , as illustrated in the left panel for $\epsilon_p = 0.01$ eV.

ences reported in Table 1, using the burst spectrum. The resulting E_r for the 34 bursts of Table 1 with known redshift ranges from 10^{52} to 10^{54} erg, with an average of $10^{53.3}$ erg for 20 bursts with known peak energy ϵ and $10^{53.0}$ erg for all 34 bursts, assuming $\epsilon = 200$ keV when not known.

The true radiative output of GRBs depends on the degree of ejecta collimation. If the optical light-curve breaks (i.e. decay steepenings) observed at 0.3–3 days in a majority of well-monitored pre-Swift bursts (e.g. Zeh, Klose & Kann 2006) are due to “jet effects” (i.e. boundary of the jet becoming visible to observer when its decreasing Lorentz factor reaches γ_j^{-1} , the inverse of the jet half-opening angle, and jet lateral spreading beginning to affect the jet dynamics at about the same time), then the epoch t_b of the light-curve break can be used to determine the jet opening θ_j :

$$\theta_j = [(t_b)^{-1}]^{1/4} = 0.096 \frac{t_{b, \text{rd}}^{1/4}}{(z+1)E_{k,53}} \text{ rad} \quad (24)$$

where t_b is measured in days and $E_{k,53}$ is the isotropic-equivalent of the jet kinetic energy after the prompt phase, measured in 10^{53} erg. The derivation of the above result for the jet dynamics (1) assumed that the jet is decelerated by its interaction with the wind produced by a Wolf-Rayet star. The post-burst jet kinetic energy is not known but can be related to the GRB bolometric output E_r by assuming a burst radiative efficiency $\epsilon_r = E_r / (E_r + E_k)$. Then the collimation-corrected initial energy of the two-sided GRB jet is

$$2E_k = \frac{1}{2} \theta_j^2 (E_r + E_k) = 10^{50.7} \frac{E_{r,53} t_{b, \text{rd}}^{1/4}}{(z+1)(1-\epsilon_r)} \text{ erg} \quad (25)$$

Monitoring of the optical emission of the GRB afterglows listed in Table 1 is somewhat limited, nearly none of the optical light-curves displaying a jet-break until the last measurement, as shown by slow optical decays $d \log F = d \log t$ listed in column 10 of Table 1 (decays faster than t^{-2} are likely to be caused by a jet-break having occurred). Evidence for jet-breaks in the X-ray afterglow light-curve, consisting of a steepening to a decay faster than t^{-2} , is not considered here because the decoupled optical and X-ray afterglow light-curve behaviours seen in many cases (e.g. chromatic X-ray light-curve breaks) suggests that sometimes these two emission arise from different mechanisms and/or parts of the relativistic outflow. Thus, for most afterglows, we have only a lower limit on t_b (column 9 in Table 1) which yields a lower limit on the initial jet energy E_k .

Figure 5 shows the distribution of the lower limits on E_k for bursts with known redshift, assuming a GRB bolometric radiative efficiency $\epsilon_r = 0.5$ (which minimizes the jet energy { equation 25) and $t_j = 1$ day whenever the available optical afterglow monitoring does not allow us to set even a lower limit on t_b . For a given burst, the jet energy is maximal for ϵ_p in the optical, as this value minimizes the synchrotron peak flux required to account for the observed optical counterpart flux, which maximizes the Compton parameter, the GeV output, and the total isotropic-equivalent burst output. The largest lower limit on the initial jet kinetic energy, obtained for $\epsilon_p = 1$ eV, is 10^{53} erg, being lower by a factor 10 for a factor 100 increase or decrease in ϵ_p .

The energy that the long-GRB progenitor (black-hole plus accretion torus formed after the collapse of a Wolf-Rayet core) can deposit into a relativistic jet depends on the available energy reservoir (a torus with a rest-mass energy $1 M_\odot c^2 = 2 \times 10^{54}$ erg and a black-hole with a comparable spin energy, for the collapsar model { Woosley 1993) and the efficiency at which the available energy is extracted and deposited into highly relativistic ejecta (e.g. magnetohydrodynamical energy extraction is limited to 5.7 percent (for a non-rotating BH) and 42 percent (for a maximally rotating BH) of the torus gravitational binding energy and up to 29 percent of the black-hole mass). In the case when the accretion rate is $0.1 M_\odot \text{ s}^{-1}$ and the black-hole spin parameter is $a = 0.95$, Popham, Woosley & Fryer (1999) obtain a maximum of $10^{52.3}$ erg for the energy of the outflow resulting from the annihilation of neutrinos and antineutrinos produced by dissipation in the torus. Using general relativistic MHD simulations of accreting tori by Kerr black-holes, Krolik, Hawley & Hirose (2005) find that, at the radius of marginal stability, the Poynting flux produced by the Blandford-Znajek mechanism carries 0.25 percent of the accreted mass-energy for $a = 0.5$, 1 percent for $a = 0.9$, rising to about 10 percent for $a = 0.998$. Similar results, showing a rapidly increasing jet efficiency as function of the BH spin parameter, are obtained by McKinney (2005), who obtains an upper limit of 6.8 percent for the jet efficiency for a maximally rotating BH, corresponding to a jet energy of $10^{53.1}$ erg, if the disk as a mass of $1 M_\odot$.

Thus, the jet energy expected in the collapsar model is less than 10^{53} erg, which implies that, if the sub-MeV emission of the GRBs listed in Table 1 was produced from upscattering of a lower energy emission, the peak energy ϵ_p of the primary spectrum could not have been in the optical for all bursts (right panel of Figure 5). Instead, if ϵ_p were

universal, the synchrotron peak energy must have been below 0.1 eV (left panel of Figure 5) or above 10 eV, to yield lower limits on the jet energy that are sufficiently below the theoretical upper limit of 10^{53} erg. Values of ν_p above 10 eV lead to even lower required jet energies but the 10 keV prompt flux could be dominated by the synchrotron emission instead of the first upscattering, thus the resulting low-energy GRB spectrum would be softer than usually observed. For this reason, we consider that only $\nu_p < 0.1$ eV is a possible solution for reducing the required jet energetics below the theoretical expectation for the collapsar model.

4 CONCLUSIONS

The occasional detection of an optical counterpart whose brightness exceeds the extrapolation of the GRB sub-MeV emission suggests that, if the two emissions arise from same medium, the burst could be the first upscattering of the synchrotron spectrum that yields the optical counterpart. We find 10 such cases in a sample of 29 bursts with optical counterpart measurements, but the true fraction of over-bright optical counterparts could be larger because half of those 29 bursts have been observed only by Swift-BAT (Table 1), which underestimates the true hardness of the GRB spectral slope below the peak energy if that peak energy fell in BAT's relatively narrow bandpass.

A straightforward expectation for the synchrotron self-Compton model for GRBs is that the upscattering of the burst photons yields a GeV-TeV prompt emission, whose brightness is found to depend strongly on the peak energy of the synchrotron spectrum. In this paper, we provided the formalism by which the GeV prompt emission from the second scattering is related to the sub-MeV emission from the first scattering and the optical emission from synchrotron, and applied that formalism to bursts with optical counterpart measurements, to estimate the expected GeV prompt fluxes, the bolometric GRB output and energetics, and the correlation of the expected GeV fluence with the burst and optical brightnesses.

The synchrotron self-Compton model can be tested in the following ways. The measurement by Fermi-LAT or Agile-GRID of the 0.1-100 GeV fluence of the emission produced during the burst by the second upscattering, combined with the properties (peak flux and energy) of the prompt burst emission produced by the first upscattering, leads to two solutions for the location of the synchrotron peak energy (equation 23). The lower energy solution corresponds to a soft optical spectrum and a hard GeV spectrum, while the higher energy solution is identified with a hard, self-absorbed optical and a soft (falling) GeV spectrum. Future multicolour measurements of the optical prompt emission obtained by fast-response telescopes and measurements of the GeV emission by high-energy satellites will allow a test of consistency between the observed optical and GeV spectra and the above-mentioned model expectations. A stronger test will be possible if the peak energy of the second scattering emission spectrum is also determined, as the GeV flux and peak energy provide two independent determinations of the synchrotron spectral peak, for given properties of the -ray spectrum (see Figure 2).

From the expected GeV output and using the con-

straints on the outflow opening set by the afterglow optical light-curve, we have calculated lower limits on the collimated radiation output and jet initial energy for 34 bursts with optical counterpart measurements and redshifts. The resulting jet energies are lower limits because one third of optical counterpart measurements are upper limits, which lead to lower limits on the GeV output, and because most of the available coverage of optical afterglows sets only lower limits on the jet-break time, leading to lower limits on the jet half-angle. Figure 5 shows that the resulting lower limits on the double-jet initial energy ranges over 2 decades, with the largest value (10^{53} erg) being obtained if the peak energy of the synchrotron spectrum is close to the optical (right panel), and with the lower limit on the jet energy decreasing by a factor 10 for a factor 100 decrease of the synchrotron peak energy (left panel). Thus, the energetics required by the synchrotron self-Compton model for GRBs and the upper limit of 10^{53} erg expected for jets produced after the core-collapse of massive stars indicate that the peak energy of the synchrotron spectrum should be often well below optical.

For the 29 bursts with optical counterparts measurements, we find that, if the unknown peak energy of the synchrotron spectrum does not have a very wide distribution, the brightness of the second inverse-Compton scattering remains correlated with the flux of the first upscattering and anticorrelated with that of the primary synchrotron spectrum. Thus, the synchrotron self-Compton model for GRBs will be invalidated if Fermi-LAT detects GeV prompt emission consistent with the extrapolation of the burst spectrum for bursts that are bright at sub-MeV energies and dim in the optical. This test of the synchrotron self-Compton model for GRBs applies only if GeV prompt photons are detected because the lack of such detections in a given burst may not necessarily imply the production of low GeV prompt fluxes, but could be due instead to the source being optically-thick to photon-photon attenuation.

ACKNOWLEDGMENTS

The author acknowledges the great help in collecting the optical counterparts measurements provided by the GR-Blog site at <http://grad40.as.utexas.edu> created by Robert Quimby and maintained together with Erin McMahon and Jeremy Murphy.

This work was supported by the US Department of Energy through the LANL/LDRD 20080039DR program.

REFERENCES

- Amati L. et al, 2002, *A & A*, 390, 81
- Amano K., Inoue S., 2007, *ApJ*, 671, 645
- Bouvier A. et al, 2008, *GCN* 8183
- Galam T. et al, 1999, *Nature*, 398, 394
- Gonzales M. et al, 2003, 424, 749
- Girardot J., Guetta D., 2003, *ApJ*, 598, L11
- van der Horst A., Goldstein A., 2008, *GCN* 8141, 8278
- Hurley K. et al, 1994, *Nature*, 372, 652
- Kaneko Y. et al, 2008, *ApJ*, 677, 1168
- Karpov S. et al, 2008, *GCN* 7558
- Krolik J., Hawley J., Hirose S., 2005, *ApJ*, 622, 1008

- Kumar P., Panaitescu A., 2008, preprint (arXiv:0805.0144)
- Lloyd N., Petrosian V., Mallozzi R., 2000, *ApJ*, 534, 227
- Mészáros P., Rees M., 1997, *ApJ*, 476, 232
- Mészáros P., Rees M., 1999, *MNRAS*, 306, L39
- McKinney J., 2005, *ApJ*, 630, L5
- Panaitescu A., Mészáros P., 2000, *ApJ*, 544, L17
- Panaitescu A., Kumar P., 2007, *MNRAS*, 376, 1065
- Papathanassiou H., Mészáros P., 1996, *ApJ*, 471, L91
- Pe'er A., Waxman E., 2004, *ApJ*, 603, L1
- Perley D. et al, 2008, *ApJ*, 672, 449
- Piran T., Sari R., Zou Y., 2008, preprint (arXiv:0807.3954)
- Popham R., Woosley S., Fryer C., 1999, *ApJ*, 518, 356
- Racusin J. et al, 2008, *Nature*, 455, 183
- Rees M., Mészáros P., 1994, *ApJ*, 430, L93
- Sari R., Piran T., 1999, *ApJ*, 517, L109
- Sommer M. et al, 1994, *ApJ*, 422, L63
- Stamatikos M. et al, 2008, preprint (arXiv:0809.2132)
- Tajima H. et al, 2008, *GCN* 8246
- Wang X., Dai Z., Lu T., 2001, *ApJ*, 556, 1010
- Woosley S., 1993, *ApJ*, 405, 273
- Yu Y., Wang X., Dai Z., 2008, preprint (arXiv:0806.2010)
- Zeh A., Klose S., Kann D., 2006, *ApJ*, 637, 889